Chemical Engineering Journal 146 (2009) 477–485

Contents lists available at ScienceDirect

Chemical Engineering Journal

journal homepage: www.elsevier.com/locate/cej

Steam reforming of dimethyl ether over $CuO–ZnO–Al_2O_3–ZrO_2$ + ZSM-5: A kinetic study

Dongmei Feng, Yuanyuan Wang, Dezheng Wang, Jinfu Wang*

Beijing Key Laboratory of Green Chemical Reaction Engineering and Technology, Department of Chemical Engineering, Tsinghua University, Beijing 100084, China

ARTICLE INFO

Article history:
Received 12 May 2008
Received in revised form 1 November 2008
Accepted 3 November 2008

Keywords:
Dimethyl ether
Steam reforming
Kinetic model
CuO–ZnO catalyst
Zeolite

ABSTRACT

Experiments were carried out to characterize the kinetics of dimethyl ether (DME) steam reforming (SR) in a fixed bed reactor catalyzed by a bifunctional catalyst comprising a physical mixture of 50:50 wt.% $CuO–ZnO–Al_2O_3–ZrO_2$ + ZSM-5 at 200–300 °C and atmospheric pressure. The influences of the feed composition (steam/DME ratio), temperature and space velocity on DME conversion, hydrogen yield and CO_2 selectivity were obtained. A kinetic model for combined DME SR based on the reaction mechanisms for methanol to DME from Park and Froment and methanol SR from Peppley et al. was used. The kinetic parameters were determined by regression using the DME conversion, hydrogen yield and CO_2 selectivity at a given steam/DME feed ratio (steam/DME molar ratio of 3.5).

1. Introduction

The polymer electrolyte fuel cell (PEFC) has come to be recognized as a highly efficient and clean power generator for both stationary and mobile applications [1,2]. Hydrogen is the fuel for this. The steam reforming (SR) of natural gas, methanol, gasoline, and dimethyl ether (DME) can be used to produce hydrogen. All these raw materials have their advantages and drawbacks. Among these, DME has the advantages of high energy density, non-toxicity, easy availability, safe handling and storage, and that the infrastructure in place for liquefied petroleum gas (LPG) distribution can be readily adapted for DME. The feasibility of producing hydrogen from a DME SR process has already been discussed [3–8].

Hydrogen production from DME SR is a two-step process. The first step is the acid catalyzed hydrolysis of DME to methanol (Eq. (1)). This is followed by methanol steam reforming over Cu or Cu/ZnO catalysts (Eq. (2)).

- DME hydrolysis:

$$CH_3OCH_3 + H_2O \rightleftarrows 2CH_3OH, \quad \Delta H_r^0 = +36.6\,\text{kJ/mol} \tag{1}$$

- MeOH steam reforming:

$$CH_3OH + H_2O \rightleftarrows CO_2 + 3H_2, \quad \Delta H_r^0 = +49.1\,\text{kJ/mol} \tag{2}$$

- DME SR, Eq. (3), is a linear combination of Eqs. (1) and (2):

$$CH_3OCH_3 + 3H_2O \rightleftarrows 2CO_2 + 6H_2, \quad \Delta H_r^0 = +135.0\,\text{kJ/mol} \tag{3}$$

The integrated system of DME SR also contains products that undergo the water gas shift (WGS) reaction:

$$CO + H_2O \rightleftarrows CO_2 + H_2, \quad \Delta H_r^0 = -41.17\,\text{kJ/mol} \tag{4}$$

Thermodynamic considerations [9,10] suggested that a high DME conversion cannot be attained when there is only DME hydrolysis to methanol. It is an equilibrium-limited reaction. However, its conversion can be increased to exceed the equilibrium limit by coupling it with methanol SR, that is, the equilibrium of reaction (1) can be shifted in the forward direction, leading to high DME conversion, if there is a simultaneous consecutive methanol conversion by its steam reforming, reaction (2). In the coupled overall DME SR reaction system, DME hydrolysis is considered the rate-limiting step. Therefore, the enhancement of DME hydrolysis conversion is an important factor in obtaining a higher DME SR conversion. The hydrolysis reaction is known to take place over an acidic catalyst. ZSM-5 is an active acidic catalyst [11,6]. In addition to ZSM-5, acidic alumina (γ-Al_2O_3) has also been used [3,12]. ZSM-5 and γ-Al_2O_3 are active for DME hydrolysis in different temperature ranges: >270 °C for γ-Al_2O_3 and 200–300 °C for ZSM-5 catalyst. It is well known that Cu–ZnO and $CuO–ZnO–Al_2O_3$ have high activity for the synthesis and steam reforming of methanol. Thus, the preferred catalyst should be a bifunctional one, e.g., comprising ZSM-5 as the DME hydrolysis catalyst and copper as the methanol steam reforming catalyst.

* Corresponding author. Fax: +86 10 62797490.
E-mail addresses: wangjf@flotu.org, wangjfu@mail.tsinghua.edu.cn (J. Wang).

1385-8947/$ – see front matter © 2008 Elsevier B.V. All rights reserved.
doi:10.1016/j.cej.2008.11.005

Nomenclature

A_i	preexponential factor of an elementary step of type i (s^{-1} bar^{-1})
C_i	concentration of surface species i (mol g-cat^{-1})
C_{H^+}	concentrations of vacant acid sites (mol g-cat^{-1})
C_{Si^+}	total surface concentration of site i (mol m^{-2})
DME	dimethyl ether
DMO^+	dimethyloxonium ion
E_i	activation energy of reaction type i (kJ mol^{-1})
F_i	molar flow rate of ith component (mol s^{-1})
F	objective function of optimization for minimizing
ΔH	heat of protonation (kJ mol^{-1})
H^+	acidic site of ZSM-5 (mol g-cat^{-1})
j_i	number of data points
K_i	equilibrium constant of an elementary step
k'_i	rate coefficient of an elementary step i
k_i	rate coefficient of step i, incorporating C_{H^+}
k_i	rate constant for reaction i (mol g-cat^{-1} s^{-1})
K_i	equilibrium constant of reaction i
L	length of reactor (m)
MeOH	methanol
$MeOH_2^+$	methoxonium ion
p_i	partial pressure of gas-phase species i (bar)
$r(i)$	reaction rate for species i (mol g-cat^{-1} s^{-1})
r_i	rate of reaction i (mol s^{-1} m^{-2})
R_i	parameters to be estimated after re-parameterization of rate and equilibrium constants
R	gas constant (8.3145 J mol^{-1} K^{-1})
R_i	rate of reaction i (mol s^{-1})
R_1^+	surface methoxy
$S(i)$	standard entropy of component i (J mol^{-1})
S_i	active site i in reaction mechanism (m^2 g^{-1})
S_i	selectivity of ith component
T	temperature (°C)
T_m	mean temperature (°C)
W	mass of catalyst (g)
x	conversion of ith component
Y_i	yield of ith component

Subscripts

Hyd	DME hydrolysis
R	methanol steam reforming
W	water–gas shift
D	decomposition
1	active site 1 when on variable S
1a	active site 1a when on variable S
2	active site 2 when on variable S
2a	active site 2a when on variable S

Superscripts

C	consumption
F	formation, used in the rate coefficient
Pr	protonation
(i)	species adsorbed on active site i where i is 1, 1a, 2 or 2a
*	composite parameter as defined in reaction equation
T	indicating total concentration of active sites

The majority of works devoted to DME SR research is the method of catalyst preparation with attention given to the use of zeolite or alumina in the catalyst studies [3,13,4,14]. The catalysts and experimental conditions used are summarized in Table 1. Some researchers [15–17] have studied the kinetics of methanol SR.

In this paper, we report experiments carried out to characterize the activity of physically mixed catalysts containing $CuO–ZnO–Al_2O_3–ZrO_2$ and ZSM-5 catalysts for DME SR in an isothermal fixed bed reactor. The influences of steam/DME ratio, space velocity and temperature in the feed gas were studied and a detailed kinetic model of DME SR was parameterized for the bifunctional catalyst.

2. Experimental

2.1. Catalyst preparation

The catalyst comprised a $CuO–ZnO–Al_2O_3–ZrO_2$ catalyst, manufactured by a novel co-precipitation procedure [18] as the catalyst component for methanol steam reforming, and a solid zeolite ZSM-5 catalyst (Si/Al = 25) purchased from the Catalyst Plant of Nankai University for DME hydrolysis. The copper-based catalyst was prepared using the corresponding nitrates as the metal sources and sodium carbonate as the precipitant. The precipitate was washed, dried, and then calcined at 350 °C for 4 h to yield the $CuO–ZnO–Al_2O_3–ZrO_2$ catalyst. In this catalyst, copper is the active phase and ZnO was added to improve the dispersion of copper and its reducibility while the addition of Al_2O_3 and ZrO_2 were used to improve the specific surface area and to reduce the sintering of the catalyst. All catalysts were ground and sieved to a particle diameter of 20–25 mesh to eliminate internal diffusion resistance. The weight ratio of the two components in the bifunctional catalyst was about 1 for $CuO–ZnO–Al_2O_3–ZrO_2$ + ZSM-5 catalyst.

2.2. Catalyst characterization

The structures of the catalysts were characterized by N_2 BET adsorption and X-ray diffraction (XRD). The BET surface area was obtained using a high resolution BET equipment described in Li et al. [19,20]. Powder XRD patterns of the catalysts were obtained with a Bruker D8 Advance type X-ray diffractometer using nickel-filtered Cu Kα radiation. The patterns were recorded for $10° < 2\theta < 90°$. To study the stability of the bifunctional catalyst, the DME conversion obtained during a continuous operation of 80 h under standard conditions was plotted as a function of time.

2.3. Equipment and reaction conditions

The experimental setup is shown in Fig. 1. In the feed section, the reactant DME and reducing gas N_2/H_2 were controlled by mass flow controllers. DME SR was carried out using an isothermal fixed bed reactor (20 mm i.d.) with the total gas space velocity of 1180–9000 ml g-cat^{-1} h^{-1}, steam/DME molar ratio of 3.5, and at atmospheric pressure. The temperature range used was 200–300 °C. Before the reaction, the catalyst was reduced with a 4% H_2/96% N_2 mixture at atmospheric pressure by raising the temperature slowly to the reaction temperature over 10 h and holding at 230 °C for 2 h. A mixture of deionized water, fed by a custom built vaporizer by means of a stratospheric piston pump, and DME gas was introduced into the reactor for reaction. The first sample of the effluent was taken 2 h after steady reaction conditions were established. Then samples were taken every 30 min for online analysis of the effluent composition by a gas chromatograph. The final result shown is the average of five data points.

Table 1
Catalyst and experimental conditions in the literature and this paper.

Copper catalyst	Solid acid catalyst	Temperature (°C)	DME conversion (%)	Literature
Cu-based spinel	γ-Al_2O_3	250–500	0–97	[3]
Copper iron spinel	H-mordenite, ZSM-5, bayerite, γ-Al_2O_3, TiO_2	200–400	2–98	[7]
Copper ferrite spinel	Al_2O_3	250–450	0–97	[8]
Pt, Pd–Al_2O_3	Al_2O_3	200–250	20–100	[14]
CuO–ZnO–Al_2O_3–ZrO_2	ZSM-5	200–300	16–100	In this paper

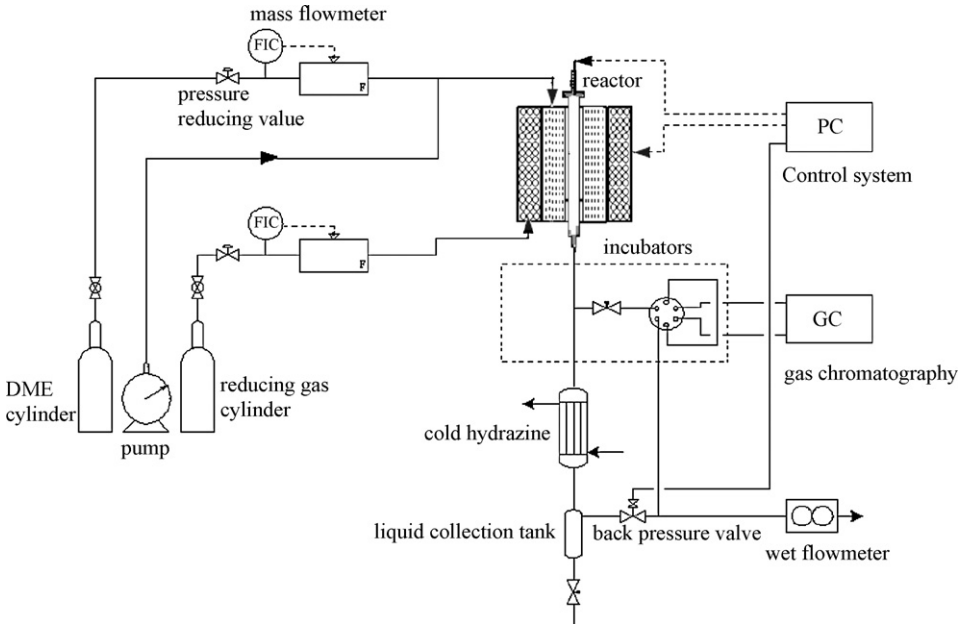

Fig. 1. Schematic view of the fixed-bed reactor system.

2.4. Product analysis

The compositions of the effluent gas were analyzed by an online gas chromatograph (GC) equipped with a TCD (VARIAN, GC–7890II). A Porapak T column was used for the separation of DME, MeOH, and H_2O, and a TDX-01 column was used for the separation of H_2, CO, and CO_2. DME conversion x and CO_2 selectivity S were defined as follows:

$$x_{DME}\ (\%) = \frac{F_{DME,in} - F_{DME,out}}{F_{DME,in}} \times 100 \quad (5)$$

$$S_{CO_2}\ (\%) = \frac{F_{CO_2}}{F_{CO} + F_{CO_2}} \times 100 \quad (6)$$

where F_{DME} and F_{CO_2} were the molar flow rates of DME and CO_2, respectively. In and out denote the inlet and outlet molar flow rates.

The hydrogen yield, a parameter used for the activity, was defined as the ratio of the molar amount of DME converted to hydrogen to the total molar amount of DME fed to the reactor. This was calculated by the following relation:

$$Y_{H_2}\ (\%) = \frac{F_{H_2}}{F_{DME,in}} \left(\frac{F_{DME,in}}{F_{H_2}} \right)_T \times 100 \quad (7)$$

where F_{H_2} was the effluent molar flow rate of H_2. $(F_{DME,in}/F_{H_2})_T = 1/6$ was the theoretical molar ratio of DME fed and H_2 produced.

3. Results and discussion

3.1. Catalyst characterization

A high surface area was found for ZSM-5, while CuO–ZnO–Al_2O_3–ZrO_2 had a low surface area. The BET surface area of ZSM-5 was 365 $m^2\ g^{-1}$, which was larger than that of CuO–ZnO–Al_2O_3–ZrO_2, 108 $m^2\ g^{-1}$.

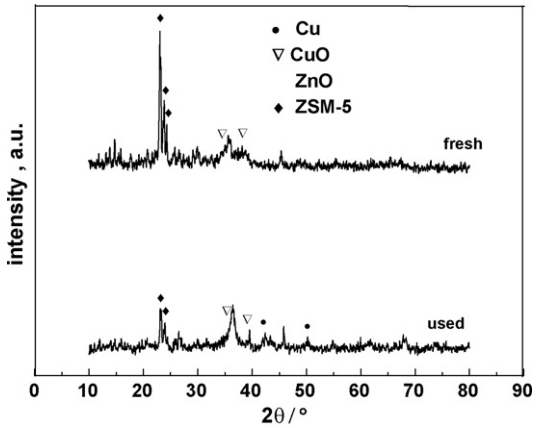

Fig. 2. XRD patterns of the physical mixtures of CuO/ZnO/Al_2O_3/ZrO_2 and ZSM-5 catalysts.

Fig. 2 shows X-ray diffractograms from physical mixtures of CuO–ZnO–Al_2O_3–ZrO_2 and ZSM-5 catalysts before and after DME steam reforming. The ZSM-5 catalysts had a sharp diffraction peaks at $2\theta = 23.0^\circ$, 23.8°, and 24.4° indicating that these had fewer defects, and a high degree of crystallinity. In the XRD patterns of the mixed catalysts, there were rather weak peaks that can be assigned to CuO, which was the main component of the CuO–ZnO–Al_2O_3–ZrO_2 catalyst. These appeared at $2\theta = 35.5^\circ$, and 38.6°. The CuO peaks overlapped the ZnO peaks at $2\theta = 36^\circ$. There were no peaks that can be assigned to Al_2O_3 and ZrO_2, indicating that Al_2O_3 and ZrO_2 existed in an amorphous or microcrystalline state. It is generally thought that DME hydrolysis actively takes place over acidic site of acid catalysts, while methanol SR proceeds over metal catalysts. The fresh CuO–ZnO–Al_2O_3–ZrO_2 catalyst was almost inactive if the catalyst was not reduced before the reaction. Also, the Cu metal peaks at 43° and 50° showed that some of the copper was present as the metallic phase on the reacted catalyst, while the fresh catalyst had no Cu metal peaks. Thus, although the XRD pattern indicated more CuO than metallic copper on the used catalyst, the active species for methanol SR reaction was assumed to be metallic copper, which is in agreement with the majority opinion that the active species for methanol synthesis is metallic copper.

From Fig. 3, it can be seen that the bifunctional catalyst of CuO–ZnO–Al_2O_3–ZrO_2 + ZSM-5 had good stability over 80 h during which the DME conversion was almost constant. However, the reaction temperature had to be limited to less than 270 °C to avoid deactivation of the copper-based catalyst caused by Cu sintering.

Figs. 4–6 show the effect of steam/DME molar ratio, temperature and space velocity on DME conversion, hydrogen yield, and CO_2 selectivity, respectively.

3.2. Effect of feed ratio (steam/DME molar ratio)

Fig. 4 shows that DME conversion and hydrogen yield increased considerably when the steam/DME ratio was increased from 3 to 7. Carbon dioxide, hydrogen and methanol were the main products with the selected bifunctional catalyst. No methyl formate and methane were present in the products at all temperatures investigated. Methane is the most thermodynamically stable product but was not produced because of the selectivity of the catalyst. In the present work, carbon monoxide was not detected at reaction temperatures lower than 240 °C except the total gas space velocities was 3935 ml g-cat^{-1} h^{-1}. Trace amount was observed only at temperatures above 240 °C along with high conversions of DME of above 60%. The DME conversion and hydrogen yield were far

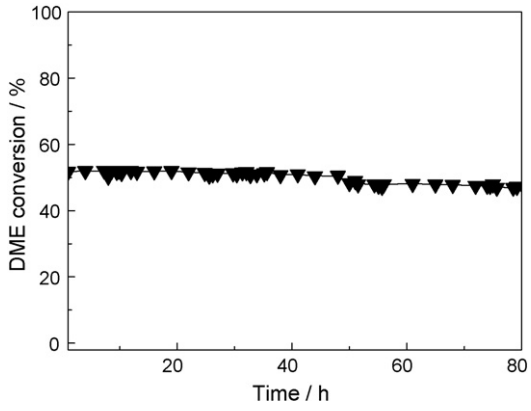

Fig. 3. DME conversion during SR of CuO–ZnO–Al_2O_3–ZrO_2 + ZSM-5 catalyst as a function of time with 1 g catalyst and n(DME)/n(H_2O) = 1/3.5, temperature = 240 °C; space velocity, 4922 ml g-cat^{-1} h^{-1}.

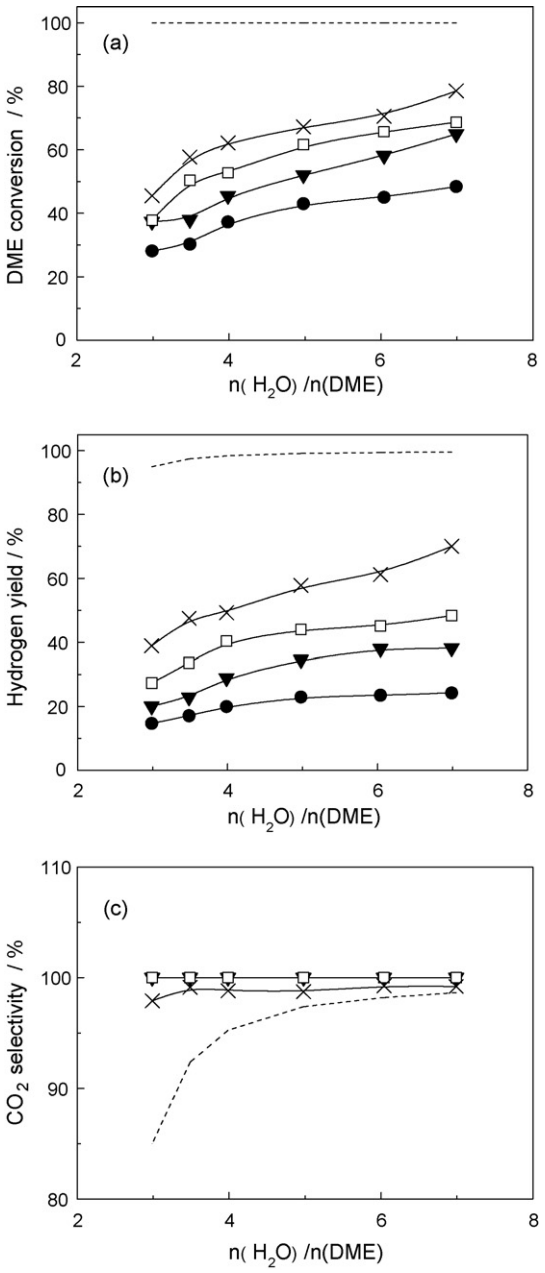

Fig. 4. Effect of steam/DME ratio on DME SR at different space velocities over CuO–ZnO–Al_2O_3–ZrO_2/ZSM-5 catalyst: (a) DME conversion, (b) H_2 yield and (c) CO_2 selectivity. The reaction conditions were: catalyst, 1 g; temperature, 240 °C. Space velocity: (—) thermodynamic equilibrium; (●) 9000 ml g-cat^{-1} h^{-1}; (▼) 6872 ml g-cat^{-1} h^{-1}; (□) 4922 ml g-cat^{-1} h^{-1}; (×) 3935 ml g-cat^{-1} h^{-1}.

from the equilibrium state even though the amount of water in the feed was more than the amount of DME. It can be seen in Fig. 4 that with increased steam/DME ratio, DME SR was accelerated, which led to higher DME conversions. Also, the increase of the steam/DME ratio shifted the equilibrium of the water gas shift reaction ($CO + H_2O = CO_2 + H_2$) in the forward direction which produced H_2 and consumed H_2O. Water gas shift is rapid over copper-based catalysts. It is favored by lower temperatures and higher concentrations of steam. Similarly to the H_2 yield, the CO yield was defined as the molar percentage of DME feed that was converted to CO. The CO yield varied between 0.5 and 0.82% at 240 °C and a total gas space velocity of 3935 ml g-cat^{-1} h^{-1}. From Fig. 4, it can be seen that the CO_2 selectivity was higher than the DME SR ther-

modynamic equilibrium value, that is, CO concentrations were well below the equilibrium value. Clearly, steam in excess of the amount required by stoichiometry effectively suppressed CO formation. It was clear that the system was not in DME SR equilibrium. A higher steam/DME molar ratio was favorable for enhancing the DME conversion and reducing the CO concentration in the product. Additionally taking the thermal load and energy supply into account, the optimum steam/DME can be recommended as 3.5.

The steam to DME ratio was kept constant at 3.5 (mol/mol) in order to lower the CO concentration by inducing a water gas shift reaction in the reformer. Experiments were carried out that vary the temperature and the space velocity in order to study the effects of the temperature and contact time on catalyst activity, hydrogen yield and CO_2 selectivity.

3.3. Effect of temperature

DME SR was studied in the temperature range from 200 to 300 °C. DME hydrolysis, water gas shift and methanol SR occurred in the reactor. The activity of the mixture of $CuO–ZnO–Al_2O_3–ZrO_2$ and ZSM-5 catalysts as evaluated by the effect of temperature at a constant space velocity on DME conversion, hydrogen yield and CO_2 selectivity is shown in Fig. 5. DME conversion and hydrogen yield increased with the temperature because DME SR reaction is a very endothermic reaction. As a result, a small increase in temperature resulted in a significant increase in conversion and hydrogen yield. The molar ratio of water to DME used in the feed was chosen slightly above the stoichiometric value to favor a higher hydrogen yield when CO was produced. DME SR began to be observable at about 200 °C and approximately 100% conversion of DME was obtained at temperatures higher than 240 °C under the above reaction conditions. DME conversion and hydrogen yield increased with the temperature, but selectivity of CO_2 decreased while the CO concentration increased. The CO yields observed were 0.74–8.19% under these operating conditions. This suggested that at higher temperatures the reverse WGS was accelerated.

Fig. 5 shows that at lower temperatures, DME conversion and hydrogen yield were far from equilibrium, but with increased reaction temperature, the difference narrowed, and at 260 °C, DME conversion and hydrogen yield were very close to equilibrium. At the same time, in the experiment's temperature range, CO_2 selectivity was higher than the equilibrium value.

3.4. Effect of space velocity

The space velocity, which is a parameter that reflected the reactor efficiency, was also tested with a steam/DME ratio of 3.5 at atmospheric pressure. The total gas space velocities from 1180 to 9000 ml g-cat^{-1} h^{-1} were used to test the catalytic behavior. Fig. 6 shows that with increased gas space velocity, DME conversion and hydrogen yield decreased and CO_2 selectivity increased. At the total gas space velocity of 1180 ml g-cat^{-1} h^{-1}, the conversion of DME was about 88% and CO_2 selectivity was 98% at 220 °C. When it was increased to 9000 ml g-cat^{-1} h^{-1}, DME conversion was decreased to 18% and CO_2 selectivity was increased to 100%.

DME can be completely converted at 270 °C with a H_2 yield (defined by Eq. (7)) greater than 90% when the total gas space velocity was less than 2461 ml g-cat^{-1} h^{-1}. At the same time, CO started to form above 240 °C and the CO content was low. When the total gas space velocity was decreased to 1180 ml g-cat^{-1} h^{-1}, the conversion by the catalysts was greatly increased. The increased amount of CO was not only caused by a more rapid reverse WGS but also by the high conversion and concentration of CO_2. The CO yields were less than 8.2% under these operating conditions. We can see that the DME steam reforming is constrained to be a low

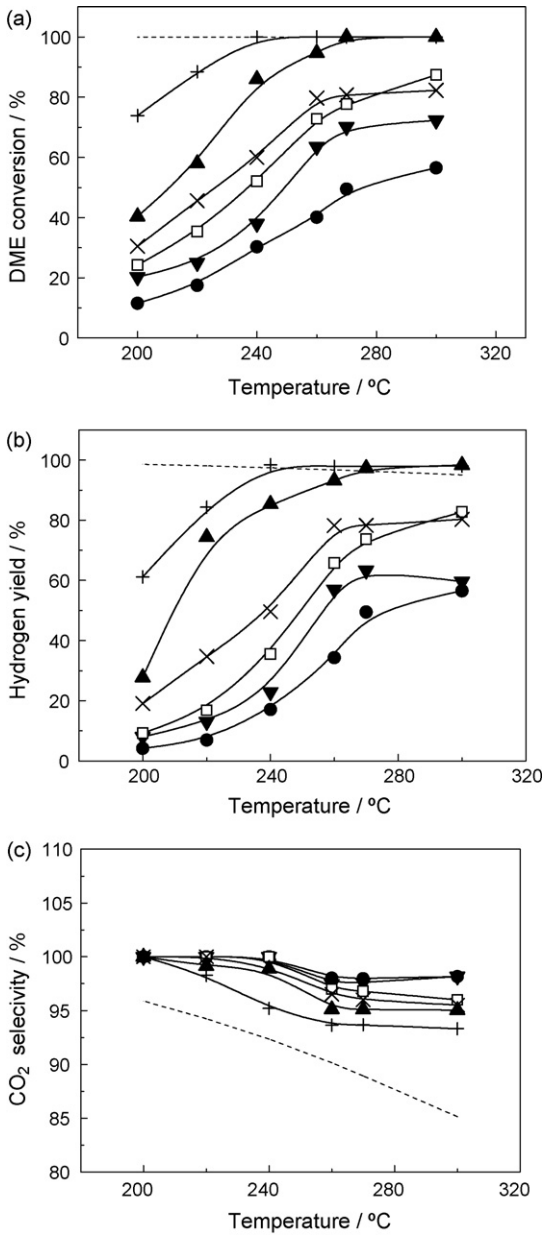

Fig. 5. Effect of temperature on DME SR over $CuO–ZnO–Al_2O_3–ZrO_2$/ZSM-5 catalyst: (a) DME conversion, (b) H_2 yield and (c) CO_2 selectivity. Catalyst, 1 g; n(DME)/n(H_2O), 1/3.5; space velocity: (—) thermodynamic equilibrium; (●) 9000 ml g-cat^{-1} h^{-1}; (▼) 6872 ml g-cat^{-1} h^{-1}; (□) 4922 ml g-cat^{-1} h^{-1}; (×) 3935 ml g-cat^{-1} h^{-1}; (▲) 2461 ml g-cat^{-1} h^{-1}; (+) 1180 ml g-cat^{-1} h^{-1}.

rate reaction by the highest temperature allowed for the Cu catalyst. The maximum allowable operating temperature for the Cu catalyst was 270 °C, which limited the rate of DME reforming because the reactor could not be operated as a higher temperature. The process needs more time to approach its equilibrium state. A low gas space velocity favors the production of H_2 in reforming of DME.

4. Kinetic analysis

4.1. Kinetic scheme

An important step to understand the catalytic behavior in DME steam reforming is to obtain the kinetics. The reaction mechanism of methanol decomposition and methanol steam reforming has

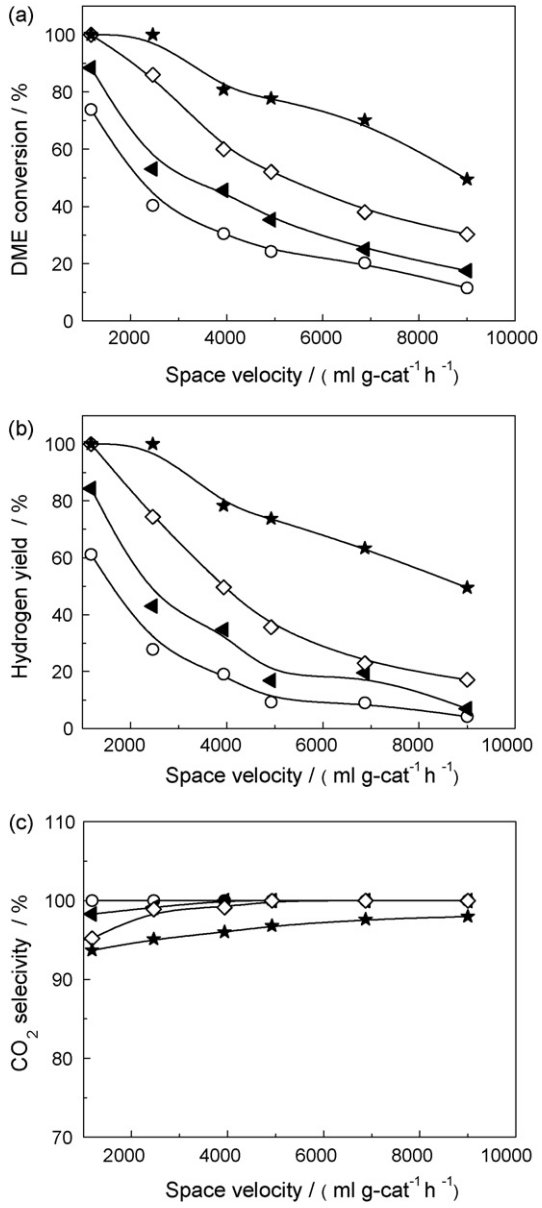

Fig. 6. Effect of space velocity on DME SR over CuO–ZnO–Al_2O_3–ZrO_2/ZSM-5 catalyst: (a) DME conversion, (b) H_2 yield and (c) CO_2 selectivity. Catalyst, 1 g; n(DME)/n(H_2O), 1/3.5; temperature: (○) 200 °C; (◂) 220 °C; (◊) 240 °C; (⋆) 270 °C.

been studied, but there is no report on the kinetics of hydrogen production from DME SR, nor studies on an integrated process of DME SR aimed at discriminating catalysts and gaining knowledge about the effects of the operating conditions. Since DME SR is the hydrolysis of DME followed by the steam reforming of methanol, in this work the kinetics of the hydrolysis of DME to methanol used the methanol dehydration to DME (its reverse reaction) elementary reaction steps in the dehydration of methanol to DME kinetic model proposed by Park and Froment [21,22]. A NMR study [23] has shown that methanol was reversibly adsorbed on Brønsted sites. The protonation was very fast on strong acidic sites and was considered to be in equilibrium. The protonated methanol thus formed led via dehydration to a surface methoxy species covalently bonded to the lattice oxygen of ZSM-5, which reacted in turn with methanol to form a dimethyloxonium ion (DMO^+). Deprotonation of the latter yielded DME and regenerated acid site. A reaction scheme for the formation of DME, written in terms of elementary steps, is given in Table 2.

Table 2
Elementary steps in the formation of DME and their related rate and equilibrium parameters [21].

Step	Elementary steps	Rate or equilibrium parameters
1	$MeOH + H^+ \rightleftarrows MeOH_2^+$	$K_{Pr,MeOH}$
2	$MeOH_2^+ \rightleftarrows R_1^+ + H_2O$	$k'_{F,R_1^+}, k'_{C,R_1^+}$
3	$R_1^+ + MeOH \rightleftarrows DMO^+$	$k'_{F,DMO^+}, k'_{C,DMO^+}$
4	$DMO^+ \rightleftarrows DME + H^+$	$\{K_{Pr,DME}\}^{-1}$

The steps for the net rate of formation of DME are steps (3) and (4). Taking DME and DMO^+ to be in equilibrium, the net rate of formation of DME can be written as

$$R_{DME} = r_{DMO^+} = k'_{F,DMO^+} C_{R_1^+} p_{MeOH} - k'_{C,DMO^+} C_{DMO^+} \quad (8)$$

In the elementary steps (1)–(4), the protonation of MeOH and DME can be taken to have reached pseudo-equilibrium, so that

$$C_{MeOH_2^+} = K_{Pr,MeOH} p_{MeOH} C_{H^+} \quad (9)$$

$$C_{DMO^+} = K_{Pr,DME}\, p_{DME} C_{H^+} \quad (10)$$

Introducing these relationships into a pseudo-steady state balance for the concentration of R_1^+ leads to

$$C_{R_1^+} = \eta'_{R_1^+} C_{H^+} \quad (11)$$

where

$$\eta'_{R_1^+} = \frac{k'_{F,R_1^+} K_{Pr,MeOH} p_{MeOH} + k'_{C,DMO^+} K_{Pr,DME} p_{DME}}{k'_{C,R_1^+} p_{H_2O} + k'_{F,DMO^+} p_{DME}} \quad (12)$$

and C_{H^+} is the concentrations of vacant acid sites.

Following Park and Froment, in order to reduce the correlation between the preexponential factor and activation energy during the regression, a mean temperature, T_m, was used to perform a re-parameterization [24] of the rate and equilibrium constants. The definitions of the parameters of the kinetic model are shown in Table 3.

Until recently, the literature on the kinetics and mechanism of methanol steam reforming on Cu–ZnO–Al_2O_3 catalysts was quite limited. An early mechanism-based kinetic model was proposed by Jiang et al. [25]. Jiang et al. used a Langmuir–Hinshelwood rate expression that was 100% selective for CO_2 and in which the rate of the WGS reaction was neglected. This model has been expanded by Peppley et al. [26,27] who gave three rate expressions: one for methanol decomposition, one for the WGS reaction and one for

Table 3
Definition of the parameters to be estimated after the re-parameterization of rate and equilibrium constants [21].

R_i	Definition
R_1	$\Delta S^0_{Pr,MeOH}/R - \Delta H^0_{Pr,MeOH}/RT_m$
R_2	$\Delta H^0_{Pr,MeOH}/R$
R_3	$\Delta S^0_{Hyd,R_1^+}/R - \Delta H^0_{Hyd,R_1^+}/RT_m$
R_4	$\Delta H^0_{Hyd,R_1^+}/R$
R_5	$\ln A_{c,R_1^+} - E_{c,R_1^+}/RTm$
R_6	$E_{c,R_1^+}/R$
R_7	$\ln A_{F,DME} - E_{F,DME}/RT_m$
R_8	$E_{F,DME}/R$
R_9	$\Delta S^0_{Pr,DME}/R - \Delta H^0_{Pr,DME}/RT_m$
R_{10}	$\Delta H^0_{Pr,DME}/R$

Table 4
Elementary reactions occurring on type 1 and type 1a sites [27].

Step	The reactions on type 1a site
5	$S_1 + S_{1a} + CH_3OH(g) \rightleftarrows CH_3O^{(1)} + H^{(1a)}$
6	$S_1 + S_{1a} + H_2O(g) \rightleftarrows OH^{(1)} + H^{(1a)}$
7	$S_1 + CO_2(g) \rightleftarrows CO_2^{(1)}$
8	$S_1 + CO(g) \rightleftarrows CO^{(1)}$
9	$2S_{1a} + H_2(g) \rightleftarrows 2H^{(1a)}$
10	$S_{1a} + CH_3O^{(1)} \rightleftarrows CH_2O^{(1)} + H^{(1a)}$
11	$CH_3O^{(1)} + CH_2O^{(1)} \rightleftarrows CH_3OCH_2O^{(1)} + S_1$
12	$CH_3OCH_2O^{(1)} + S_{1a} \rightleftarrows CH_3OCHO^{(1)} + H^{(1a)}$
13	$CH_3OCHO^{(1)} + OH^{(1)} \rightleftarrows HCOOH^{(1)} + CH_3O^{(1)}$
14	$HCOOH^{(1)} + S_{1a} \rightleftarrows H^{(1a)} + HCOO^{(1)}$
15	$OH^{(1)} + CO^{(1)} \rightleftarrows HCOO^{(1)} + S_1$
16	$HCOO^{(1)} + S_{2a} \rightleftarrows H^{(1a)} + CO_2^{(1)}$

Table 5
Elementary reactions occurring on type 2 and type 2a sites [27].

Step	The reactions on type 2a site
17	$S_2 + S_{2a} + CH_3OH(g) \rightleftarrows CH_3O^{(2)} + H^{(2a)}$
18	$S_2 + CO(g) \rightleftarrows CO^{(2)}$
19	$2S_{2a} + H_2(g) \rightleftarrows 2H^{(2a)}$
20	$CH_3O^{(2)} + S_{2a} \rightleftarrows CH_2O^{(2)} + H^{(2a)}$
21	$CH_3O^{(2)} + CH_2O^{(2)} \rightleftarrows CH_3OCH_2O^{(2)} + S_2$
22	$CH_3OCH_2O^{(2)} + S_{2a} \rightleftarrows CH_3OCHO^{(2)} + H^{(2a)}$
23	$CH_3OCHO^{(2)} \rightleftarrows CH_3OCHO(g) + S_2$
24	$CH_3OCHO^{(2)} + S_2 \rightleftarrows CH_3O^{(2)} + CHO^{(2)}$
25	$CHO^{(2)} + S_{2a} \rightleftarrows CO^{(2)} + H^{(2a)}$

methanol steam reforming, respectively. They verified the applicability of their model by fitting reaction data from a series of kinetic experiments to their model.

Peppley et al. derived the Langmuir–Hinshelwood rate laws from 12 elementary reactions and two different active sites. The H_2 adsorption site associated with the active phase for the methanol steam reaction and WGS reaction was designated as a type 1a site and the H_2 adsorption site for the second active phase was designated as a type 2a site. Elementary reactions occurring on type 1a site and type 2a site are presented in Tables 4 and 5.

Steps (11), (15) and (20) were assumed to be the rate determining steps, and the expressions for the rate of methanol synthesis, water gas shift and methanol decomposition reaction were obtained as follows:

- Methanol SR reaction:

$$r_R = \frac{k_R K^*_{CH_3O^{(1)}}(p_{CH_3OH}/p_{H_2}^{1/2})(1 - p_{H_2}^3 p_{CO_2}/K_R p_{CH_3OH} p_{H_2O}) C_{S_1}^T C_{S_{1a}}^T}{(1 + K^*_{CH_3O^{(1)}}(p_{CH_3OH}/p_{H_2}^{1/2}) + K^*_{HCOO^{(1)}} p_{CO_2} p_{H_2}^{1/2} + K^*_{OH^{(1)}}(p_{H_2O}/p_{H_2}^{1/2}))(1 + K^{1/2}_{H^{(1a)}} p_{H_2}^{1/2})} \quad (13)$$

- WGS reaction:

$$r_W = \frac{k^*_W K^*_{OH^{(1)}}(p_{CO} p_{H_2O}/p_{H_2}^{1/2})(1 - p_{H_2} p_{CO_2}/K_W p_{CO} p_{H_2O}) C_{S_1}^{T^2}}{(1 + K^*_{CH_3O^{(1)}}(p_{CH_3OH}/p_{H_2}^{1/2}) + K^*_{HCOO^{(1)}} p_{CO_2} p_{H_2}^{1/2} + K^*_{OH^{(1)}}(p_{H_2O}/p_{H_2}^{1/2}))^2} \quad (14)$$

- Methanol decomposition reaction:

$$r_D = \frac{k_D K^*_{CH_3O^{(2)}}(p_{CH_3OH}/p_{H_2}^{1/2})(1 - p_{H_2}^2 p_{CO}/K_D p_{CH_3OH}) C_{S_2}^T C_{S_{2a}}^T}{(1 + K^*_{CH_3O^{(2)}}(p_{CH_3OH}/p_{H_2}^{1/2}) + K^*_{OH^{(2)}}(p_{H_2O}/p_{H_2}^{1/2}))(1 + K^{1/2}_{H^{(2a)}} p_{H_2}^{1/2})} \quad (15)$$

4.2. Kinetics modeling

The exit partial pressure of each component was determined by numerically integrating a one-dimensional isothermal PFR model.

Table 6
Regression parameters for the DME hydrolysis kinetic model.

Parameter	Simulated
R_1	−0.9
R_2	-8.3×10^3
R_3	−4.2
R_4	-4.1×10^3
R_5	30.8
R_6	6.0×10^3
R_7	6.5
R_8	1.5×10^3
R_9	-0.3×10^2
R_{10}	-4.8×10^4

The steady state mass balance for the ith component was:

$$\frac{dF_i}{dl} = R_i \frac{W}{L} \quad (16)$$

where F_i was the molar flow rate of the ith component, W the catalyst weight (g), R_i the generation rate of the ith component (mol g-cat^{-1} s^{-1}) and L is the length of reactor (m).

A fourth-order Runge–Kutta method was used to solve the differential equation [Eq. (16)] of the kinetic model and kinetic parameters were fitted by a least-squares method. The parameters to be optimized were the kinetic constants and activation energies, and the objective function was the sum of square residuals:

$$\text{minimize} \left\{ M = \sum_{j=1}^{N} [(x_{DME,exp} - x_{DME,cal})^2 + (Y_{H_2,exp} - Y_{H_2,cal})^2 + (S_{CO_2,exp} - S_{CO_2,cal})^2] \right\} \quad (17)$$

In the expression, M is the objective function of the minimization, N is the number of data points (20), $x_{DME,exp}$ the experimental conversion of DME, $x_{DME,cal}$ the calculated conversion of DME, $Y_{H_2,exp}$ the experimental yield of H_2, $Y_{H_2,cal}$ the calculated yield of H_2, $S_{CO_2,exp}$ the experimental yield of CO_2 and $S_{CO_2,cal}$ the calculated yield of CO_2.

The objective function M was a simple multi-response objective function with equal weighing for the conversion, hydrogen yield, and selectivity. There was no attempt made to include covariances between these response variables although it was probably incorrect to consider these as uncorrelated because the optimization software could give a good fit to the data.

There are six gas species: DME, CH_3OH, H_2O, CO_2, CO, and H_2 in the DME SR system, and three elements: C, H, and O, so the

Table 7
Regression parameters for methanol steam reforming kinetic model.

Rate constant or equilibrium constant	ΔS_i (J mol^{-1} K^{-1})	k_i^{∞} (m^2 s^{-1} mol^{-1})	ΔH_i (kJ mol^{-1})	E (kJ mol^{-1})
k_R	–	7.5×10^{15}	–	123.7
$K^*_{CH_3O^{(1)}}$ (bar$^{-0.5}$)	−6.0	–	−6.5	–
$K^*_{OH^{(1)}}$ (bar$^{-0.5}$)	−60.1	–	−11.3	–
$K_{H^{(1a)}}$ (bar$^{-0.5}$)	−100.8	–	−1.0	–
$K^*_{HCOO^{(1)}}$ (bar$^{-1.5}$)	179.2	–	100.0	–
k^*_W (m^2 s^{-1} mol^{-1})	–	6.3×10^{13}	–	94.5

Table 8
Thermodynamic parameters for methanol steam reforming kinetic model.

Parameter	Simulated
$C^T_{S_1}$ (mol m^{-2})	1.3×10^{-4}
$C^T_{S_{1a}}$ (mol m^{-2})	2.0×10^{-6}
C_{H^+} (mol kg^{-1})	7.6×10^{-7}
S_A (m^2 kg^{-1})	3.2×10^5

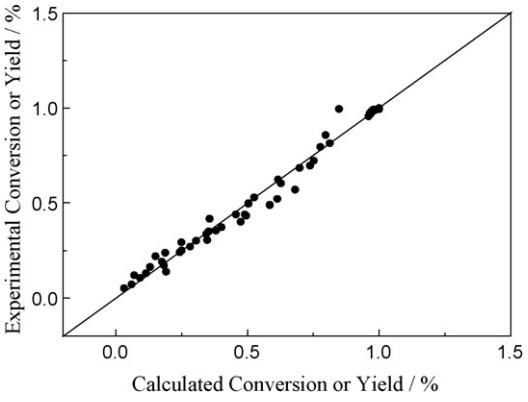

Fig. 7. Comparison of the model and experimental results.

number of independent reaction is 3. The reaction system can be expressed by DME hydrolysis, steam reforming of methanol and water–gas shift reaction. We selected reactions (1), (2) and (4) as the independent reactions, with Eqs. (8), (13) and (14) as the kinetic expressions. The optimized kinetic parameters are listed in Tables 6–8. Confidence limits for the parameters in Tables 6 and 7 were not determined because the software used could not compute these for non-linear models. The calculated DME conversion, H_2 yield and CO_2 selectivity compared with experimental results are shown in Fig. 7. The correlation coefficient of the experimental and calculated value was 0.9963.

The formula $\Delta G^{\circ}_T = -RT \ln K_p$, was used to calculate the equilibrium constant at different temperatures using basic thermodynamic data for the DME SR system reaction. The results are shown in Table 9. In Table 9, K_{Hyd}, K_R and K_W are the equilibrium constants of DME hydrolysis, methanol steam reforming and water gas shift. The equilibrium constants show how their conversions can be affected by the temperature and were also used in Eqs. (8), (13) and (14).

Table 9
Equilibrium constant for possible reactions in DME steam reforming system.

Equilibrium constant	200 °C	220 °C	240 °C	260 °C	270 °C
K_{Hyd}	3.0×10^{-2}	3.8×10^{-2}	4.7×10^{-2}	5.8×10^{-2}	6.4×10^{-2}
K_R	1.1×10^4	2.0×10^4	3.5×10^4	5.8×10^4	7.4×10^4
K_W	2.4×10^2	1.6×10^2	1.1×10^2	7.5×10^1	6.4×10^1

5. Reaction pathway

DME hydrolysis in the temperature range from 200 to 300 °C over a solid catalyst such as a ZSM-5 catalyst without the presence of a CuO–ZnO–Al_2O_3–ZrO_2 catalyst only produced methanol as the product, and DME conversion and methanol yield were very low (at 300 °C the conversion of DME was approximately 20%). With the bifunctional CuO–ZnO–Al_2O_3–ZrO_2 + ZSM-5 catalyst, hydrogen and CO_2 were the main products, with some CO and methanol. Thermodynamic calculations [9,10] showed that the equilibrium conversion of DME hydrolysis to methanol (Eq. (1)) is only 20% at 275 °C, indicating that a high DME conversion cannot be attained in a reactor where by the hydrolysis of DME was the only reaction. The addition of the Cu-based catalyst was necessary to increase DME conversion by its catalysis of methanol decomposition to continually remove methanol. From the result above, the WGS reaction also played an important role in the DME SR process. From the result above, the WGS reaction clearly played an important role in the DME SR process, converting CO into CO_2. In general, the CO concentration was significantly less than equilibrium for all conditions studied. The equilibrium of the WGS reaction was strongly influenced by the temperature, with lower temperatures favoring CO_2 and H_2 formation. It was observed that CO was only formed at high DME conversion and high temperature.

6. Conclusion

A bifunctional CuO–ZnO–Al_2O_3–ZrO_2 + ZSM-5 catalyst was used to catalyze DME steam reforming. High DME conversion, hydrogen yield and CO_2 selectivity were obtained at 200–300 °C. The reaction kinetics for the three reactions in DME steam reforming (DME hydrolysis, methanol steam reforming and reverse water gas shift) and the 26 kinetics parameters in the reaction expressions for the three reactions in DME SR (DME hydrolysis, methanol steam reforming and reverse water gas shift) were obtained from 20 sets of experimental data by regression. Simulation results showed good agreement with the experimental results. The results of this study are useful for the design, optimization and control of a DME fuel reformer system.

Acknowledgement

The authors gratefully acknowledge the financial support by the Chinese Ministry of Science and Technology (no. 2005CB221405).

References

[1] T. Isono, S. Suzuki, M. Kaneko, Y. Akiyama, Y. Miyake, I. Yonezu, Development of a high-performance PEFC module operated by reformed gas, J. Power Sources 86 (2000) 269–273.
[2] S. Ahmed, M. Krumpelt, Hydrogen from hydrocarbon fuels for fuel cells, Int. J. Hydrogen Energy 26 (2001) 291–301.
[3] Y. Tanaka, R. Kikuchi, T. Takeguchi, K. Eguchi, Steam reforming of dimethyl ether over composite catalysts of γ-Al_2O_3 and Cu-based spinel, Appl. Catal. B: Environ. 57 (2005) 211–222.

[4] K. Faungnawakij, Y. Tanaka, N. Shimoda, T. Fukunaga, S. Kawashima, R. Kikuchi, K. Eguchi, Influence of solid-acid catalysts on steam reforming and hydrolysis of dimethyl ether for hydrogen production, Appl. Catal. A: Gen. 304 (2006) 40–48.
[5] T.A. Semelsberger, K.C. Ott, R.L. Borup, H.L. Greene, Generating hydrogen-rich fuel-cell feeds from dimethyl ether (DME) using Cu/Zn supported on various solid-acid substrates, Appl. Catal. A: Gen. 309 (2006) 210–223.
[6] T. Kawabata, H. Matsuoka, T. Shishido, D. Li, Y. Tian, T. Sano, K. Takehira, Steam reforming of dimethyl ether over ZSM-5 coupled with $Cu/ZnO/Al_2O_3$ catalyst prepared by homogeneous precipitation, Appl. Catal. A: Gen. 308 (2006)82–90.
[7] T.A. Semelsberger, K.C. Ott, R.L. Borup, H.L. Greene, Generating hydrogen-rich fuel-cell feeds from dimethyl ether (DME) using physical mixtures of a commercial $Cu/Zn/Al_2O_3$ catalyst and several solid-acid catalysts, Appl. Catal. A: Gen. 65 (2006) 291–300.
[8] K. Faungnawakij, Y. Tanaka, N. Shimoda, T. Fukunaga, S. Kawashima, R. Kikuchi, K. Eguchi, Hydrogen production from dimethyl ether steam reforming over composite catalysts of copper ferrite spinel and alumina, Appl. Catal. B: Environ. 74 (2007) 144–151.
[9] T.A. Semelsberger, R.L. Borup, Thermodynamic equilibrium calculations of dimethyl ether steam reforming and dimethyl ether hydrolysis, J. Power Sources 152 (2005) 87–96.
[10] K. Faungnawakij, R. Kikuchi, K. Eguchi, Thermodynamic analysis of carbon formation boundary and reforming performance for steam reforming of dimethyl ether, J. Power Sources 164 (2007) 73–79.
[11] V.V. Galvita, G.L. Semin, V.D. Belyaev, V.A. Semilolenov, P. Tsiakaras, V.A. Sobyanin, Production of hydrogen from dimethyl ether, Appl. Catal. A: Gen. 216 (2001) 85–90.
[12] T.A. Semelsberger, K.C. Ott, R.L. Borup, H.L. Greene, Generating hydrogen-rich fuel-cell feeds from dimethyl ether (DME) using physical mixtures of a commercial $Cu/Zn/Al_2O_3$ catalyst and several solid-acid catalysts, Appl. Catal. B: Environ. 286 (2005) 11–22.
[13] K. Faungnawakij, R. Kikuchi, T. Matsui, T. Fukunaga, K. Eguchi, A comparative study of solid acids in hydrolysis and steam reforming of dimethyl ether, Appl. Catal. A: Gen. 333 (2007) 114–121.
[14] Y. Yamada, T. Mathew, A. Ueda, S. Hiroshi, K. Tetsuhiko, A novel DME steam-reforming catalyst designed with fact database on demand., Appl. Surf. Sci. 252 (2006) 2593–2597.
[15] J. Agell, H. Birgersson, M. Boutonnet, Steam reforming of methanol over a $Cu/ZnO/Al_2O_3$ catalyst: a kinetic analysis and strategies for suppression of CO formation, J. Power Sources 106 (2002) 249–257.
[16] M.P. Harold, B. Nair, G. Kolios, Hydrogen generation in a Pd membrane fuel processor: assessment of methanol-based reaction systems, Chem. Eng. Sci. 58 (2003) 2551–2571.
[17] J. Agrell, H. Birgersson, M. Boutonnet, Steam reforming of methanol over a $Cu/ZnO/Al_2O_3$ catalyst: a kinetic analysis and strategies for suppression of CO formation, J. Power Sources 106 (2002) 249–257.
[18] X. An, J.L. Li, Y.Z. Zuo, Q. Zhang, D.Z. Wang, J.F. Wang, A Cu/Zn/Al/Zr fibrous catalyst that is an improved CO_2 hydrogenation to methanol catalyst, Catal. Lett. 118 (2007) 264–269.
[19] F.X. Li, Y. Wang, D.Z. Wang, Electrochemical characterization of carbon nanotubes as electrode in electrochemical double-layer capacitors, Carbon 40 (2002) 1193–1197.
[20] D.Z. Wang, F. Wei, J.F. Wang, US Patent 6,981,426 (January 2006).
[21] T.Y. Park, G.F. Froment, Kinetic modeling of the methanol to olefins process. 1. Model formulation, Ind. Eng. Chem. Res. 40 (2001) 4172–4186.
[22] T.Y. Park, G.F. Froment, Analysis of fundamental reaction rates in the methanol-to-olefins process on ZSM-5 as a basis for reactor design and operation, Ind. Eng. Chem. Res. 43 (2004) 682–689.
[23] M.W. Anderson, P.J. Barrie, J. Klinowski, ^1H magic-angle-spinning studies of the adsorption of alcohols on molecular sieve catalyst, J. Phys. Chem. 95 (1991) 235–240.
[24] J.R. Kitrell, Mathematical modeling of chemical reactions, Adv. Chem. Eng. 8 (1970) 97–103.
[25] C.J. Jiang, D.L. Trimm, M.S. Wainwright, Kinetic study of steam reforming of methanol over copper-based catalysts, Appl. Catal. A: Gen. 97 (1993) 245–255.
[26] B.A. Peppley, J.C. Amphlett, L.M. Kearns, R.F. Mann, Methanol-steam reforming on $Cu/ZnO/Al_2O_3$. Part 1. The reaction network, Appl. Catal. A: Gen. 197 (1999) 21–29.
[27] B.A. Peppley, J.C. Amphlett, L.M. Kearns, R.F. Mann, Methanol-steam reforming on $Cu/ZnO/Al_2O_3$ catalysts. Part 2. A comprehensive kinetic model, Appl. Catal. A: Gen. 197 (1999) 31–49.